PROBABILISTIC CAPACITY AND SEISMIC DEMAND MODELS AND FRAGILITY ESTIMATES FOR REINFORCED CONCRETE BUILDINGS BASED ON THREE-DIMENSIONAL ANALYSES

BY

HAO XU

THESIS

Submitted in partial fulfillment of the requirements
for the degree of Master of Science in Civil Engineering
in the Graduate College of the
University of Illinois at Urbana-Champaign, 2014

Urbana, Illinois

Advisor:

Professor Paolo Gardoni

ABSTRACT

This thesis presents bivariate fragility estimates for reinforced concrete (RC) buildings accounting for their three-dimensional (3D) response to earthquake ground motions conditioning on spectral accelerations in the two planar directions. The fragility estimates are conducted using the demand and capacity models typically for the 3D responses. The demand models expressed in terms of drift are developed as functions of the spectral accelerations in the two planar directions. The demand prediction is compared in a probabilistic framework with the capacity estimates. The proposed capacity models for five performance levels consider the strength and stiffness degradation under the bi-axial loading. The proposed approach for the fragility estimate considers the uncertainties involved in the spectral acceleration components and capacity variation. The proposed approach is illustrated considering a typical 3-story RC building and results are compared with those from a traditional two-dimensional approach. The results indicate that the two-dimensional approach tends to significantly underestimate the fragility.

ACKNOWLEDGEMENT

First I would like to thank my advisor Prof. Paolo Gardoni, who gave me lots of help during my work on this thesis. I am really grateful for the suggestions and encouragement he gave me on both my research and my daily life.

I am very grateful for the help from all my friends in the MAE center. Their diligence motivates me to keep optimistic and work hard. It is my honor to have the chance to work with them together. Thank all the professors and friends who always help me, both here and in China. They help me improve a lot during the last two years of my stay in the US.

Finally I would like to thank my parents and my grandparents, for their care and encouragement. It is their love on me that helps me overcome all the challenges here.

TABLE OF CONTENTS

CHAPTER 1 INTRODUCTION 1

CHAPTER 2 PROPOSED FORMULATION OF DRIFT DEMAND MODEL FOR 3D RESPONSE OF RC BUILDINGS 4

CHAPTER 3 DRIFT DEMAND MODEL FOR TYPICAL THREE-STORY RC BUILDING . 7

CHAPTER 4 PROPOSED DRIFT CAPACITY MODEL FOR 3D RESPONSE OF RC COLUMNS 24

CHAPTER 5 THREE-DIMENSIONAL FRAGILITY ESTIMATES 28

CONCLUSION 38

REFERENCES 40

CHAPTER 1

INTRODUCTION

1.1 Background and Past Work Review

Most existing studies on the seismic reliability of buildings are based on two-dimensional (2D) analyses. Examples include, Hwang et al. [1], Erberik and Elnashai [2], Ramamoorthy et al. [3, 4]; Ellingwood et al. [5]; Celik and Ellingwood [6]; and Bai et al. [7]. Hwang et al. [1] developed estimates of the reliability of planar frame structures subject to the in-plane earthquake excitation. Erberik and Elnashai [2] studies the seismic reliability of the flat-slab structure. Ramamoorthy et al. [3, 4]; Ellingwood et al. [5]; Celik and Ellingwood [6]; and Bai et al. [7] studied the reliability of non-seismic designed reinforced concrete (RC) buildings. This study shows that reliability estimates based on 2D analysis tend to be inaccurate even for the symmetric buildings.

More recently a few studies have started to look at the reliability of buildings based on three-dimensional (3D) analysis. For example, Schotanus et al. [8] developed a response surface to consider the different failure modes of the structure under bi-axial loadings. Jeong and Elnashai [9] proposed a spatial index to evaluate the 3D structural response. Aziminejad and Moghadam [10] studied the effect of different types of eccentricities on the reliability estimates. However, while they carried out 3D time-history analysis, the reliability was only expressed in terms of a single intensity measure. This study finds that it is important to compute the reliability of buildings considering the intensity measures in both planar directions.

1.2 Objective and Scope

This study develops probabilistic seismic demand and capacity models based on the 3D response of a typical three-story RC building. The demand models are functions of two horizontal spectral accelerations, which consider the effects of both two horizontal ground motion components on the structural response. Capacity models proposed for five performance levels take into account the strength and stiffness degradation due to bi-axial loadings. Then bivariate fragility estimates are developed for the considered RC building, based on the proposed demand and capacity models. Finally, this paper compares the results from the proposed 3D fragility analysis with those from the traditional 2D fragility analysis.

1.3 Outline

This thesis is organized in 5 chapters:

Following the introduction, Chapter 2 provides the general formulations of the drift demand model for 2D and 3D response of the RC building.

Chapter 3 develops the drift demand models based on the 2D and 3D structural response of a typical three-story RC frame building.

Chapter 4 builds the drift capacity model considering the 3D structural response of the given RC building.

Chapter 5 conducts the bivariate fragility estimates on the RC building based on the proposed

demand and capacity models. This section also compares the results from the 2D and 3D fragility analyses.

CHAPTER 2

PROPOSED FORMULATION OF DRIFT DEMAND MODEL FOR 3D RESPONSE OF RC BUILDINGS

2.1 Formulation of Drift Demand Model for 2D Response of RC Buildings

This paper uses the definition of seismic demand given by Wen et al. [11] as the maximum inter-story drift (δ_D) of a building subject to an earthquake ground motion. Ramamoorthy et al. [3] defined the following linear model that relates the natural logarithm of δ_D with the natural logarithm of the spectral acceleration at the building fundamental period S_a:

$$\ln(\delta_D) = \theta_0 + \theta_1 \ln(S_a) + \sigma\varepsilon \tag{2.1}$$

where $\boldsymbol{\theta} = (\theta_0, \theta_1)$ are unknown model parameters; $\sigma\varepsilon$ is the model error [12]; σ is the unknown standard deviation of the model error; ε is a normal random variable with zero mean and unit standard deviation. The unknown parameters $\boldsymbol{\Theta} = (\boldsymbol{\theta}, \sigma)$ were estimated using virtual data so that the model is overall unbiased. However, Ramamoorthy et al. [3] showed that the lineal model form in Eq. (2.1) tends to underestimate δ_D for small and large values of S_a, and to overestimate δ_D for intermediate values of S_a.

To overcome this local bias, Ramamoorthy et al. [3] proposed a bilinear model that can be written as

$$\begin{aligned} \ln(\delta_D) &= \theta_0 + \theta_1 \ln(S_a) + \sigma_1\varepsilon_1, \text{ when } \ln(S_a) \le \theta_{S_a} \\ \ln(\delta_D) &= \theta_0 + \theta_1\theta_{S_a} + \theta_2\left[\ln(S_a) - \theta_{S_a}\right] + \sigma_2\varepsilon_2, \text{ when } \ln(S_a) > \theta_{S_a} \end{aligned} \tag{2.2}$$

where $\boldsymbol{\theta} = (\theta_0, \theta_1, \theta_2, \theta_{S_a})$ are unknown model parameters; $\sigma_1\varepsilon_1$ and $\sigma_2\varepsilon_2$ are the model errors for the two portions of the model; σ_1 and σ_2 are the corresponding unknown standard deviations; ε_1 and ε_2 are corresponding normal random variables with zero mean and unit standard deviation. Comparing Eqs. (2.1) and (2.2) we see that θ_2 is the slope of the second part of the bilinear model. The models in Eqs. (2.1) and (2.2) are functions of only one spectral acceleration and can only be used for two-dimensional (2D) analysis. However, they do not account for the bi-axial loading in a three-dimensional (3D) analysis.

2.2 Formulation of Drift Demand Model for 3D Response of RC Buildings

To account for the bi-axial loading in 3D analysis, we proposed to use a model form proposed by Simon et al. [13] for 3D analysis. Simon et al. [13] generalized Eq. (2.1) as

$$\ln\left(\delta_{Dk}\right) = \theta_{0k} + \theta_{1k}\ln\left(S_{ak}\right) + \sigma_k\varepsilon \tag{2.3}$$

where $k = [x, y]$; δ_{Dk} is the maximum inter-story drift in the direction k from a 3D analysis; S_{ak} is the spectral acceleration at the fundamental period in direction k; $\boldsymbol{\theta}_k = (\theta_{0k}, \theta_{1k})$ are unknown model parameters; $\sigma_k\varepsilon$ is the model error; σ_k is the unknown standard deviation of the model error. Similarly, they generalized Eq. (2.2) as

$$\begin{aligned} \ln\left(\delta_{Dk}\right) &= \theta_{0k} + \theta_{1k}\ln\left(S_{ak}\right) + \sigma_{1k}\varepsilon_1, \text{ when } \ln\left(S_{ak}\right) \le \theta_{S_ak} \\ \ln\left(\delta_{Dk}\right) &= \theta_{0k} + \theta_{1k}\theta_{S_ak} + \theta_{2k}\left[\ln\left(S_{ak}\right) - \theta_{S_ak}\right] + \sigma_{2k}\varepsilon_2, \text{ when } \ln\left(S_{ak}\right) > \theta_{S_ak} \end{aligned} \tag{2.4}$$

where $\boldsymbol{\theta}_k = (\theta_{0k}, \theta_{1k}, \theta_{2k}, \theta_{S_ak})$ are unknown model parameters; $\sigma_{1k}\varepsilon_1$ and $\sigma_{2k}\varepsilon_2$ are the model errors for the two portions of the model; σ_{1k} and σ_{2k} are the corresponding unknown standard deviations.

Based on the relationship between δ_{Dk} and S_{ak} given above, the following total demand model is used to predict the logarithm of the maximum inter-story drift $\ln(\delta_D)$:

$$\delta_{SRSS} = \sqrt{\delta_{Dx}^2 + \delta_{Dy}^2}$$
$$\ln\left(\delta_D\right) = \theta_{0D} + \theta_{1D} \ln\left(\hat{\delta}_{SRSS}\right) + \sigma_D \varepsilon \tag{2.5}$$

where $\boldsymbol{\theta} = (\theta_{0D}, \theta_{1D})$ are unknown model parameters; $\hat{\delta}_{SRSS}$ is the point estimate of δ_{SRSS} using the medians of δ_{Dx} and δ_{Dy} obtained from Eq. (2.3) or (2.4); $\sigma_D \varepsilon$ is the model error; σ_D is the unknown standard deviation of the model error. In this study, we develop a probabilistic drift demand model for the 3D response of RC buildings using the model form in Eqs. (2.4) and (2.5).

CHAPTER 3

DRIFT DEMAND MODEL FOR TYPICAL THREE-STORY RC BUILDING

3.1 Building Configuration and Design

This study considers a typical three-story RC building designed according to the non-seismic provisions of ACI-318 [14] shown in Figure 3.1. The structural configuration is the same as the one considered in Ramamoorthy et al. [4] , which is a typical configuration for non-seismic designed low-rise buildings in Mid-America. The building is a three-story four-bay frame structure. The column spacing is 8m and the height of each story is 3.65m. The design loading for the building includes: (1) the self-weight of the structure; (2) the superimposed dead load (958 pa); (3) the cladding load (3,650 pa); and (4) the live load (2,400 pa). Beams are designed as T-section beams based on the design loading and ACI-318 [14] code. The height is 600 mm for the complete beam and 200 mm for the flange. The web width is 400 mm and the flange width is 2 m for interior beams and 1 m for exterior beams. The beam section uses 5 and 2 bars of 22 mm diameter (#7 U.S. bar), as the top and bottom reinforcement, respectively. In addition, 10mm-diameter stirrups are placed in the beams at a spacing of 400 mm. Columns are designed as 400 mm square columns. The column reinforcement uses 4 bars of 25 mm diameter (#8 U.S. bars). The arrangement of stirrups in the columns is the same as in the beams.

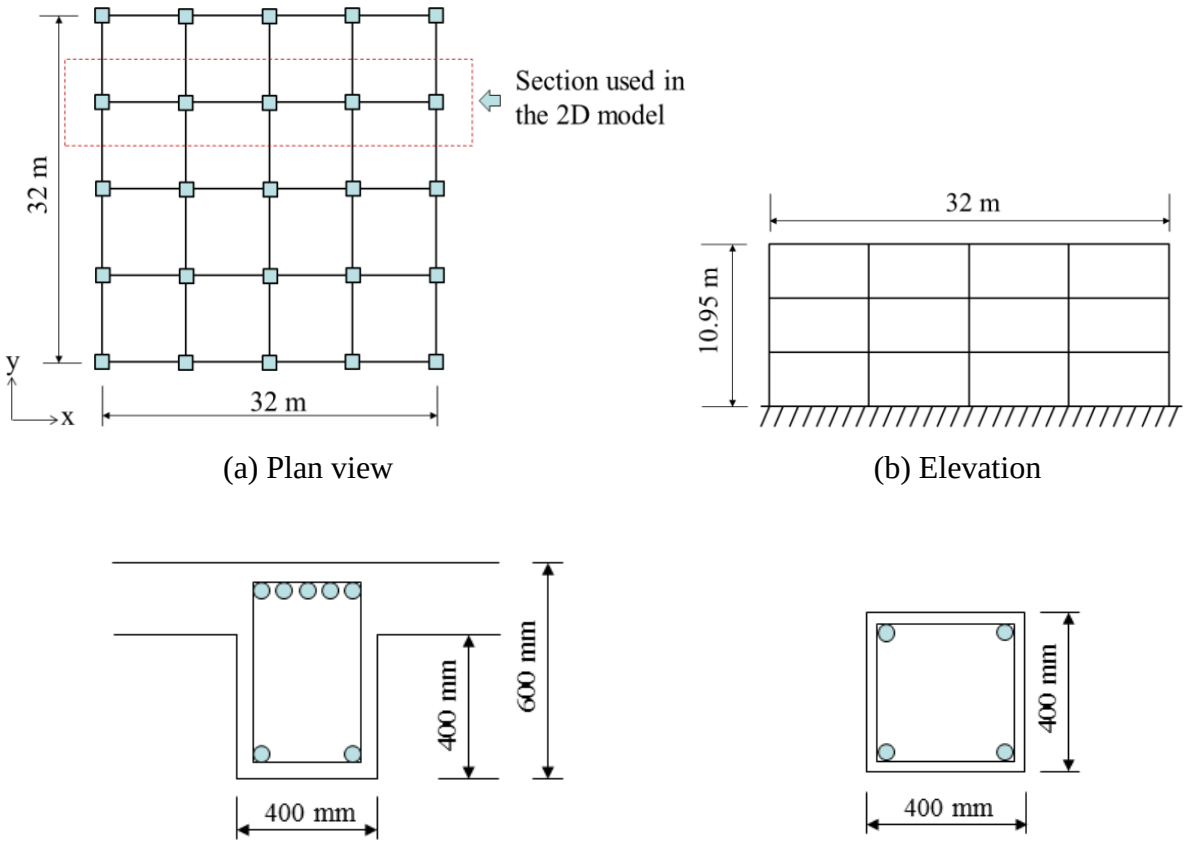

Figure 3.1 Building configuration

3.2 Structural Model

The finite element model is built and analyzed in OpenSees [15]. The model uses Concrete01 and Steel01 models for concrete and steel materials, respectively. Beam and column sections are divided into fibers to show the different properties of unconfined concrete, confined concrete and reinforcing bars. The members are modeled as nonlinear beam column elements, which can capture the actual distribution of the plastic region along the members. This study constructs both 2D and 3D models of the building to compare the results from 2D and 3D time history analysis.

The 2D model is obtained by considering an interior frame in one direction of the building. Gravity analyses are carried out first to find the fundamental periods of the building models. The fundamental periods (*T*) of the 2D and 3D models are 0.89s and 0.87s, respectively. Values of two periods are close to each other since the building is symmetric.

3.3 Ground Motion Records

We considered 200 ground motion sets (each set including records in two orthogonal directions) from the Pacific Earthquake Engineering Research Center (PEER) database [16] . The selection was based on Shome and Cornell [17]. The ground motion records are divided into 5 bins and the characteristics for each bin are given below:

(1) Bin-I (SMSR: small M and small R): M= [5.5-6.5], R= [15-30] km.

(2) Bin-II (SMLR: small M and large R): M= [5.5-6.5], R= [30-50] km.

(3) Bin-III (LMSR: large M and small R): M= [6.5-7.5], R= [15-30] km.

(4) Bin-IV (LMLR: large M and large R): M= [6.5-7.5], R= [30-50] km.

(5) Bin-V (NF: near field): M= [6.0-7.5], R= [0-15] km.

where M is the magnitude and R is the closest distance between the site and the epicenter. For each bin, half of the record sets are selected from one soil type (i.e., rock and shallow soil) and half from a second soil type (i.e., deep soil), which follows the approach given by Abrahamson and Silva [18]. Figure 3.2 and Figure 3.3 compare the median pseudo spectral acceleration (PSA) derived from the collected records and the ones from the attenuation law given by Abrahamson

and Silva [18] for two soil types, respectively. Figure 3.4 shows the comparison between the corresponding standard deviation. It can be seen that the selected records satisfy the attenuation law well, for both the median spectra and the standard deviation. This suggests that the records used in this paper can represent the characteristics of the possible ground motions. Based on the selected records, the 5% damped elastic response spectral accelerations at the structural fundamental period S_{ax} and S_{ay} are taken as the ground motion intensity measures for 3D analyses (only S_a for 2D analyses).

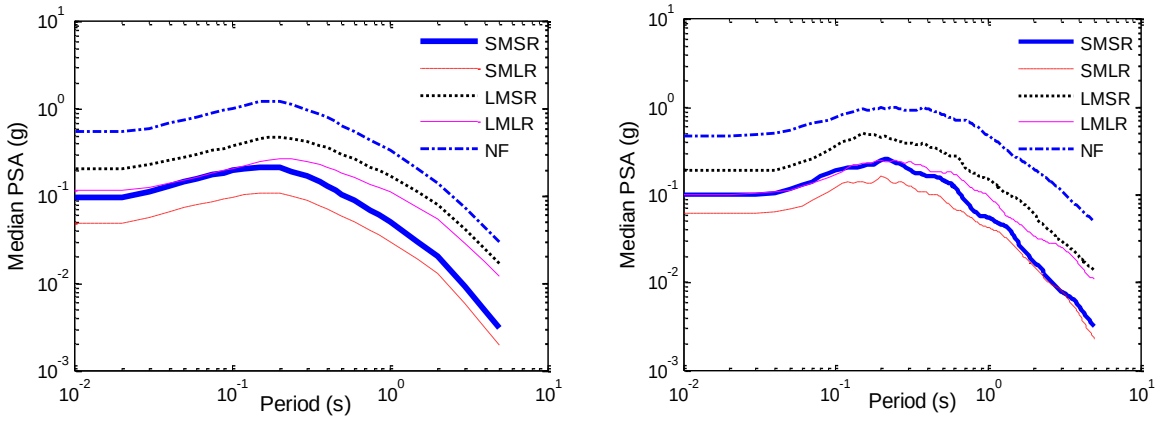

(a) Based on attenuation law (b) Based on ground motion records

Figure 3.2 Median PSA for each ground motion bin on rock and shallow soil site

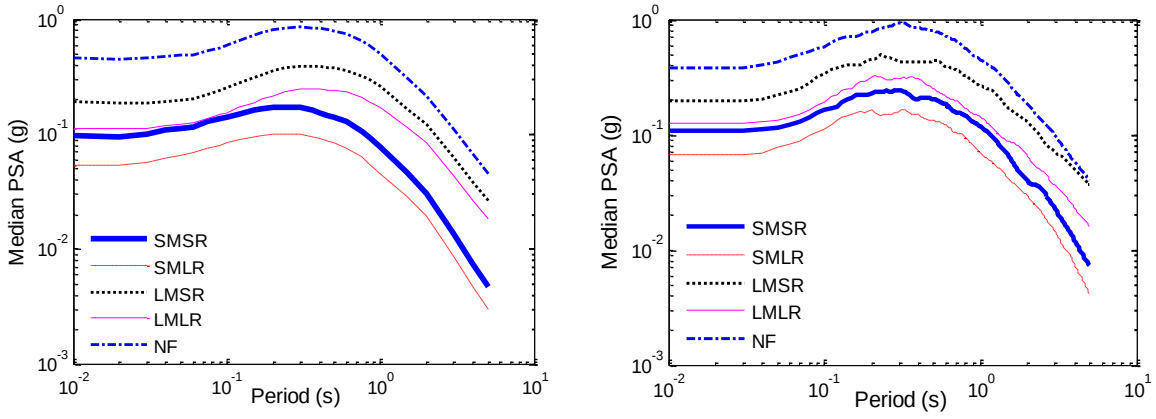

(a) Based on attenuation law (b) Based on ground motion records

Figure 3.3 Median PSA for each ground motion bin on deep soil site

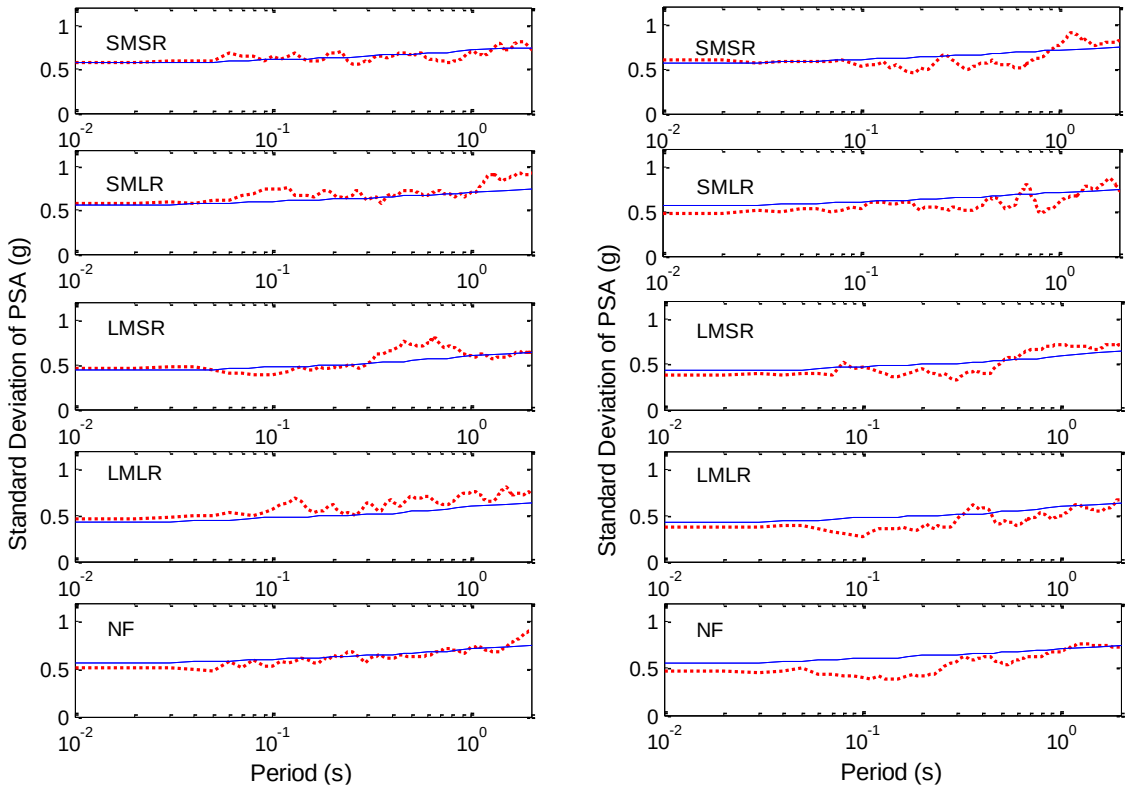

(a) Rock and shallow soil site (b) Deep soil site

Figure 3.4 Standard deviation comparison (solid lines are based on the attenuation law; dots are based on the selected ground motion records)

3.4 Structural Response

The structural response is determined by time history analyses using OpenSees [15]. The maximum inter-story drift δ_D among the three stories is taken as the demand measure. Previous work conducted 2D time history analyses to obtain δ_D for the symmetric buildings. This study conducts 3D time history analyses to investigate whether a 2D analysis is sufficient or not. We consider the following two variables that might influence whether the results from the 2D analysis are close to the ones from a 3D analysis:

(1) $\varphi_1 = \dfrac{\max(S_{ax}, S_{ay})}{\min(S_{ax}, S_{ay})}$

(2) $\varphi_2 = \left(\dfrac{\Delta t}{0.5T}\right) - floor\left(\dfrac{\Delta t}{0.5T}\right)$

where Δt is the time delay between the occurrence of the peak ground motion accelerations in the two planar directions: PGA_x and PGA_y; and $floor(\ )$ gives the nearest integer less than or equal to the number within the bracket. Physically, φ_1 captures the ratio between the larger spectral acceleration and smaller spectral acceleration in the two planar directions at the fundamental period T. As a result, a value of $\varphi_1 \approx 1$ indicates that the spectral accelerations in the two planar directions are approximately the same. In this case, the results from the 3D analysis are expected to differ from those from a 2D analysis. A value of $\varphi_1 >> 1$ indicates that the spectral acceleration in one direction is significantly larger than the one in its orthogonal direction. In this case, the results from the 3D analysis are expected to be similar to those from a 2D analysis.

On the other hand, φ_2 captures the degree of separation between the peak acceleration in each of the two planar directions. A value of $\varphi_2 \approx 0$ or $\varphi_2 \approx 1$ indicates that the peak acceleration in each of the two planar directions occur approximately at the same time. A value of $\varphi_2 \approx 0.5$ indicates the peak acceleration excitation in one direction corresponds to a negligible excitation in its orthogonal direction.

A sine wave acceleration is used as the ground motion input to study the effect of φ_1 and φ_2, on the structural response. The sine wave is defined as:

$$Acc_k = A_k \sin[\Omega(t + \Delta t_k)] \tag{3.1}$$

where, in each direction k, Acc_k is the acceleration input; A_k is the acceleration amplitude; Ω is the natural frequency of the acceleration input; t is the time; Δt_k is the time delay of the occurrence of the peak acceleration with respect to a zero-phase input.

In this case, the spectral acceleration at the fundamental period S_{ak} is determined by the ground motion acceleration amplitude A_k. So we redefine $\varphi_1 \cong \dfrac{\max(A_x, A_y)}{\min(A_x, A_y)}$. This section gives three examples to show the effect of φ_1 and φ_2 on the structural response. The acceleration inputs for the three cases are:

Case 1: $Acc_x = \sin\left[\dfrac{2\pi}{T}(t)\right]$ and $Acc_y = \sin\left[\dfrac{2\pi}{T}(t)\right]$;

Case 2: $Acc_x = \sin\left[\dfrac{2\pi}{T}(t)\right]$ and $Acc_y = \sin\left[\dfrac{2\pi}{T}(t + 0.25T)\right]$;

Case 3: $Acc_x = \sin\left[\dfrac{2\pi}{T}(t)\right]$ and $Acc_y = 2\sin\left[\dfrac{2\pi}{T}(t)\right]$.

In Case 1, $\varphi_1 = 1$ and $\varphi_2 = 0$. In Case 2, $\varphi_1 = 1$ and $\varphi_2 = 0.5$. In Case 3, $\varphi_1 = 2$ and $\varphi_2 = 0$.

Figures 3.5 to 3.7 show the results from the time history analyses for the three cases, respectively. In each figure, plot (a) shows the acceleration time history curves. Three acceleration time history curves are provided from the top to bottom, with respect to *x*, *y* direction and the total acceleration inputs, respectively. The star sign ($*$) represents the maximum acceleration in each direction. Plot (b) in each of the Figures 3.5 to 3.7 shows the drift time history curves. Three drift time history

curves are provided from the top to bottom, with respect to *x*, *y* direction and the total drift, respectively. The star sign ($*$) represents the maximum drift in each direction. Finally, plot (c) in each of the Figures 3.5 to 3.7 shows the drift path in terms of δ_x and δ_y. The dashed lines show the plan view of the first story of the building. The star sign ($*$) in each plot represents the maximum total drift.

From the plots (b) and (c) in Figure 3.5, it can be seen that the maximum drifts in *x* and *y* directions are the same. The maximum total drift from the 3D analysis in this case is much larger than the one from the 2D analysis. This is because the acceleration amplitudes in *x* and *y* directions are the same, while the peak accelerations occur simultaneously. In this case, a 3D analysis is necessary. From the plots (b) and (c) in Figure 3.6, it can be seen that the maximum drifts in *x* and *y* directions are also the same. But the maximum total drift from the 3D analysis is almost the same as the one from the 2D analysis. This is because even the acceleration amplitude in *x* and *y* directions are the same, the occurrence of the peak acceleration in one direction corresponds to a negligible acceleration in its orthogonal direction. In this case, a 2D analysis is sufficient. From the plots (b) and (c) in Figure 3.7, it can be seen that the maximum drift in *x* direction is significantly smaller than the one in *y* direction, and the maximum total drift is close to the maximum drift in *y* direction. This is because the acceleration amplitude in *x* direction is significantly smaller than the one in *y* direction. In this case, a 2D analysis is also sufficient.

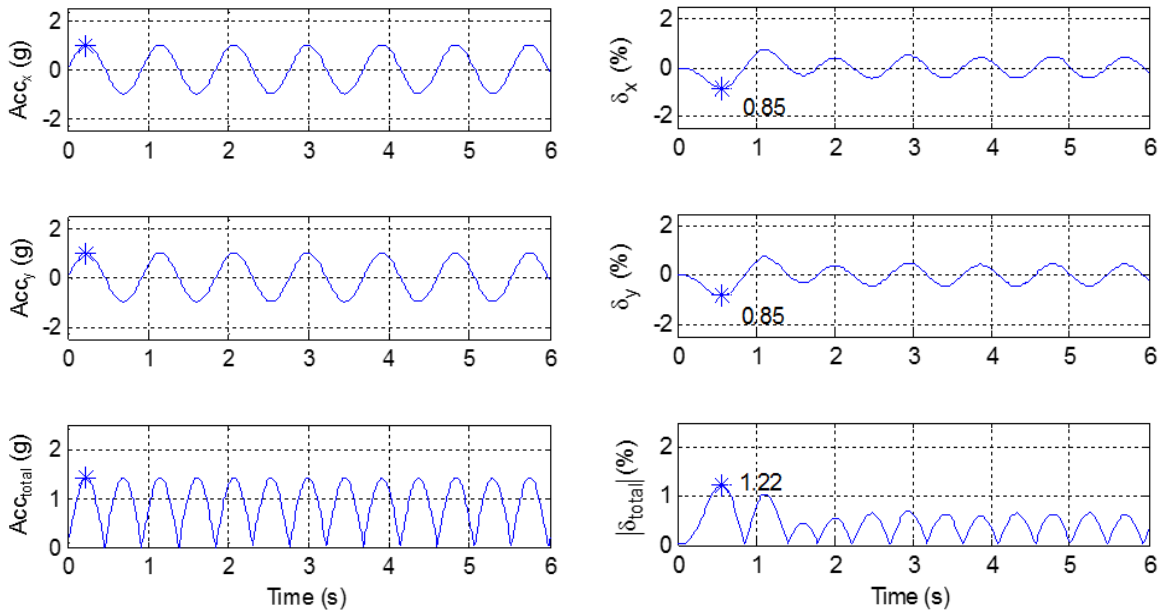

(a) Acceleration time history curves (b) Drift time history curves

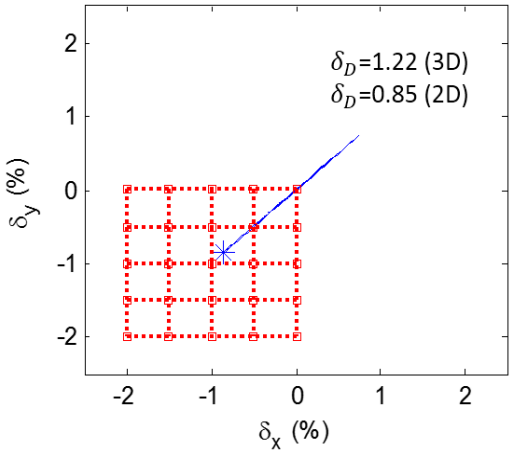

(c) First story plan view and the drift path

Figure 3.5 Time history analysis result for Case 1

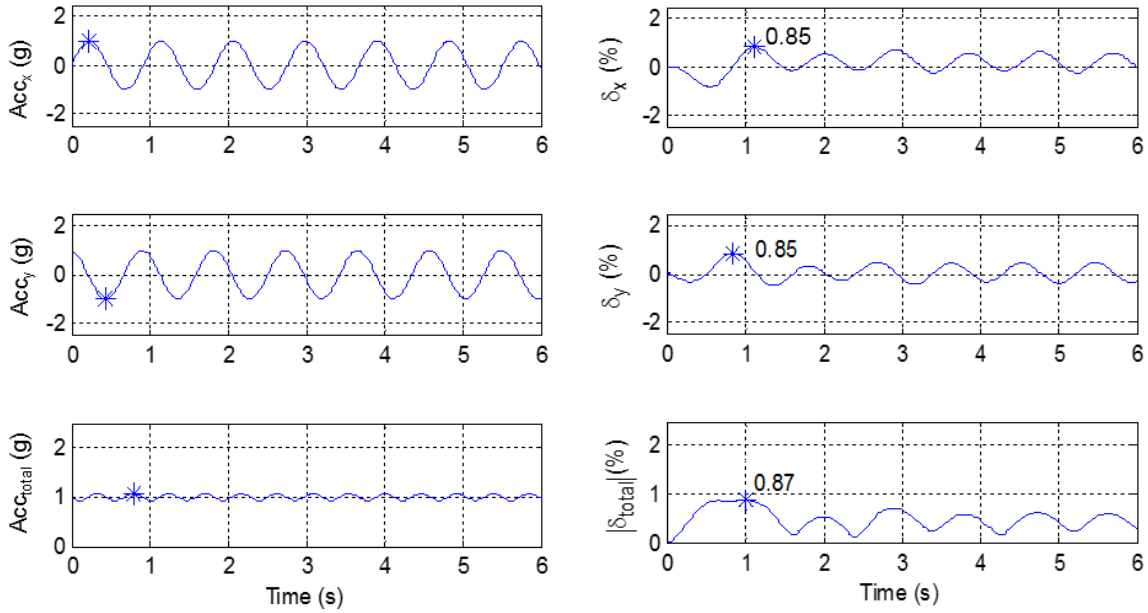

(a) Acceleration time history curves (b) Drift time history curves

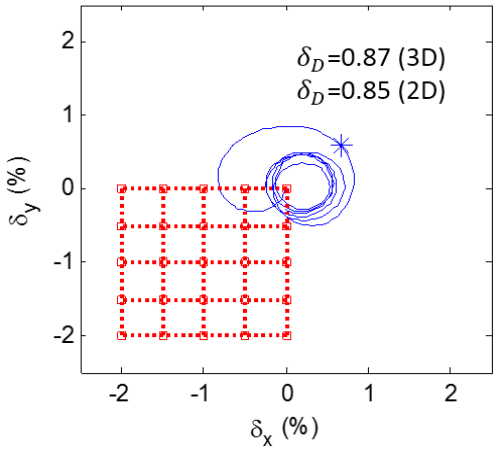

(c) First story plan view and the drift path

Figure 3.6 Time history analysis result for Case 2

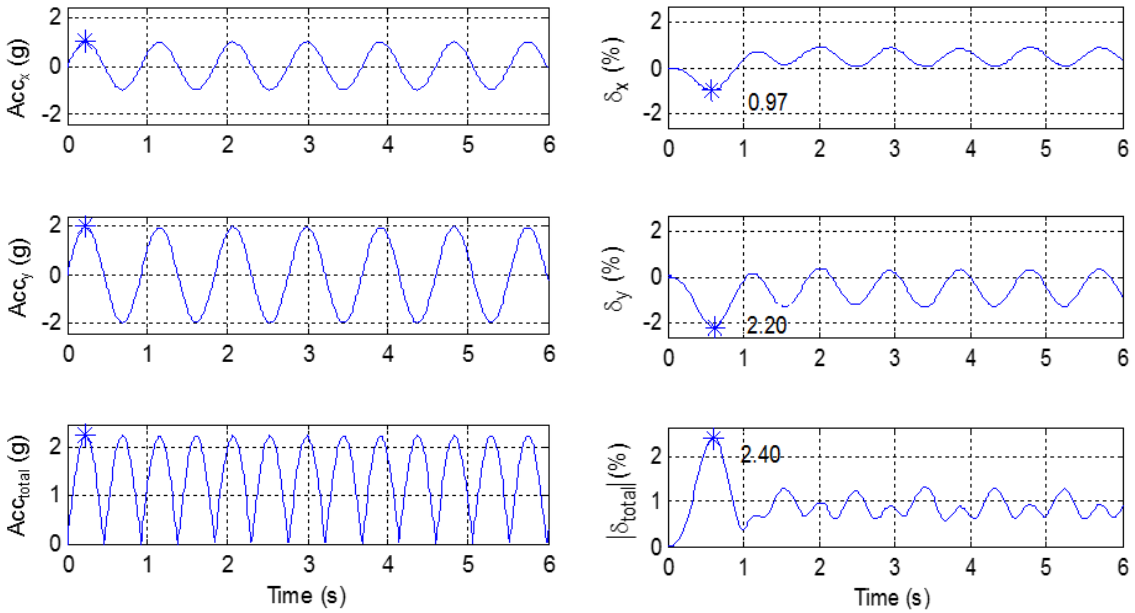

(a) Acceleration time history curves (b) Drift time history curves

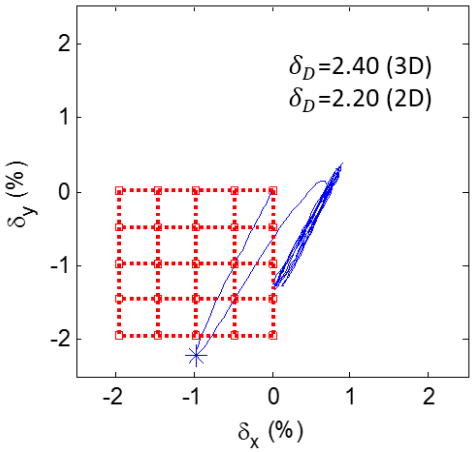

(c) First story plan view and the drift path

Figure 3.7 Time history analysis result for Case 3

This study gives an example using the real ground motions to show the effect of changing φ_1 when φ_2 remains the same and equal to approximately 0.25. Specifically, Figure 3.8 provides the acceleration time history and drift paths of the 1st story under two ground motion sets with different φ_1 ($\varphi_1 >> 1$ and $\varphi_1 \approx 1$), and similar φ_2. In the plots of drift paths, "$*$"and "●" are the location of δ_D from 3D and 2D analysis, respectively. Figure 3.9 shows the corresponding time history of the drift in the x-direction (δ_x), y-direction (δ_y), and the total drift response ($|\delta_{total}|$) of the 1st

story. The 1st story is shown because it generally experiences large drifts than the other stories. It can be seen that in the first case ($\varphi_1 >> 1$), the structural response in the y-direction is significantly larger than the response in the x-direction, and as a result the δ_D's from the 2D and 3D analysis are very close to each other. In the second case ($\varphi_1 \approx 1$), the responses in the two directions are comparable in magnitude and make a contribution to the total response. As a result, the δ_D from the 3D analysis is much larger than δ_D from the 2D analysis. As shown in this example, a 2D analysis might not be adequate to evaluate the response even of symmetric buildings. Therefore, this paper conducts 3D time history analyses for symmetric buildings to obtain δ_D.

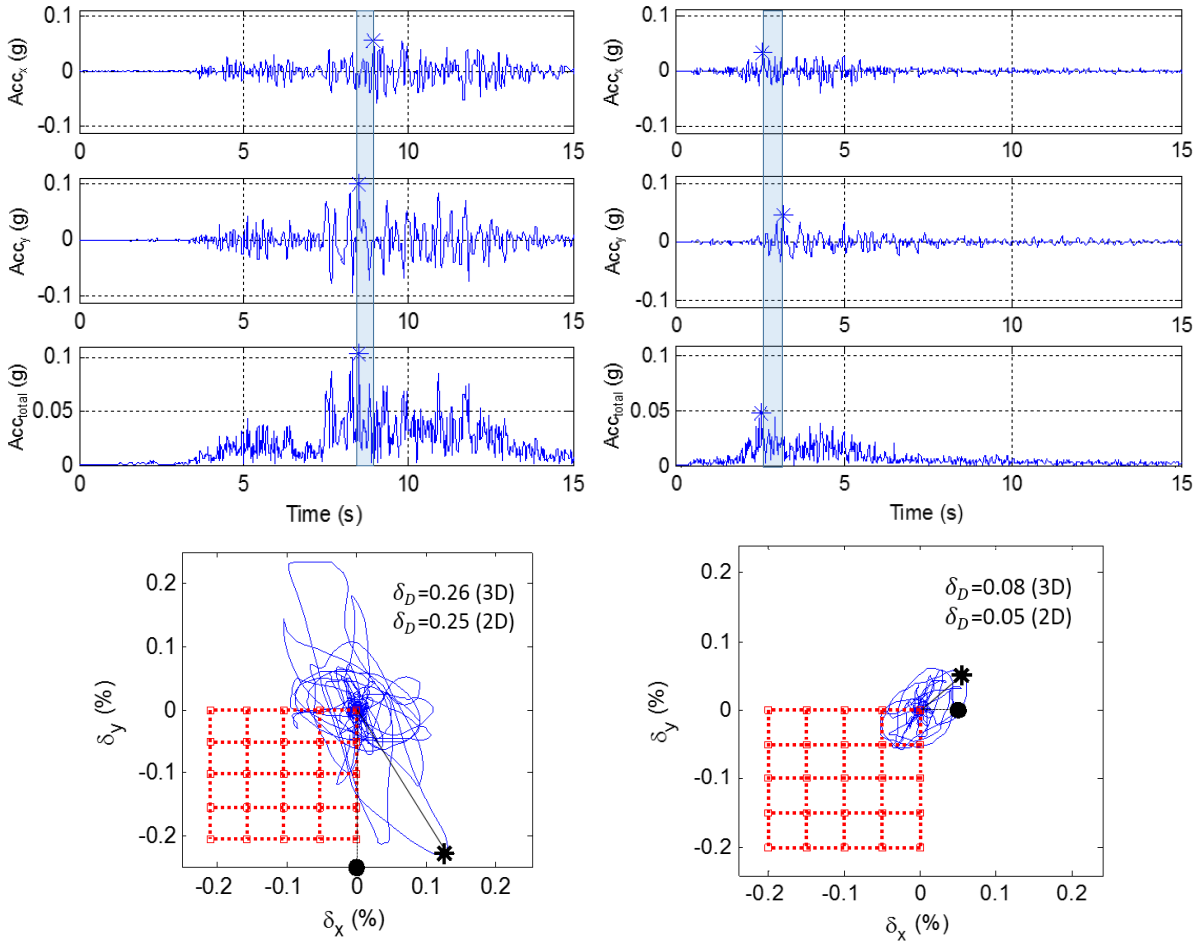

(a) when $\varphi_1 = 1.40$ and $\varphi_2 = 0.25$ (b) when $\varphi_1 = 1.04$ and $\varphi_2 = 0.26$

Figure 3.8 Acceleration time history and drift path of the 1st floor

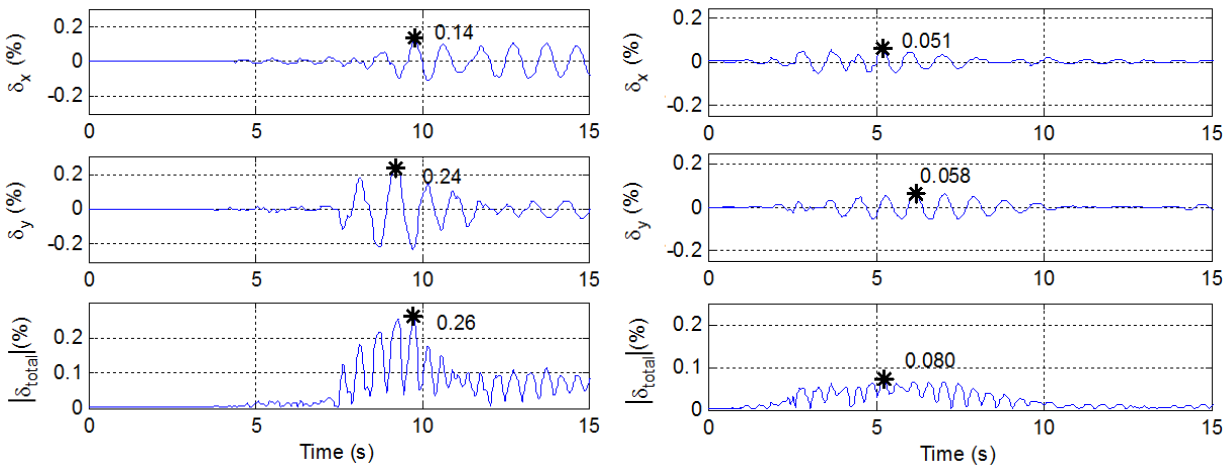

(a) when $\varphi_1 = 1.40$ and $\varphi_2 = 0.25$ (b) when $\varphi_1 = 1.04$ and $\varphi_2 = 0.26$

Figure 3.9 Drift time history of the 1st floor in each direction
("*" is the location of the maximum drift in each direction)

3.5 Model Calibration

The response data are then used to estimate the parameters $\boldsymbol{\Theta}$ using the Bayesian updating rule [19]:

$$f(\boldsymbol{\Theta}) = \gamma L(\boldsymbol{\Theta})\, p(\boldsymbol{\Theta}) \tag{3.2}$$

where $f(\boldsymbol{\Theta})$ is the posterior distribution of $\boldsymbol{\Theta}$, which reflects the updated knowledge about $\boldsymbol{\Theta}$; γ is a normalizing factor; $L(\boldsymbol{\Theta})$ is the likelihood function which captures the objective information on $\boldsymbol{\Theta}$ in the response data; $p(\boldsymbol{\Theta})$ is the prior distribution that reflects the knowledge about $\boldsymbol{\Theta}$ available before obtaining the response data. Since no prior knowledge about $\boldsymbol{\Theta}$ is available, a non-informative prior is selected.

Due to the lack of experiment data verification of the time history analysis, response quantities corresponding to a drift larger than 5% are questionable. As a result, when writing $L(\boldsymbol{\Theta})$, data

with inter-story drifts larger than 5% are categorized as "lower bound" data (i.e., $\delta_D > 5\%$). The likelihood function is then written as [12]:

$$L(\boldsymbol{\theta},\sigma) \propto \prod_{equality\ data} p\left[\sigma\varepsilon_i = r_i(\boldsymbol{\theta})\right] \times \prod_{lower\ bound\ data} p\left[\sigma\varepsilon_i > r_i(\boldsymbol{\theta})\right] \tag{3.3}$$

where $r_i(\boldsymbol{\theta})$ is the residual between the measured and the predicted demands.

This paper uses the Markov Chain Monte Carlo (MCMC) [20] method to obtain the posterior distribution of the unknown parameters in the demand models. For the 2D analysis, Table 3.1 provides the posterior statistics of the unknown parameters in the bilinear model (i.e., Eq. (2.2)). Figure 3.10 shows the predicted drift where the dots (•) and the open circles (○) show the measured logarithm of the maximum drift, corresponding to $\ln(S_a) \le \theta_{S_a}$ and $\ln(S_a) > \theta_{S_a}$, respectively. The thick line represents the mean prediction $E[\ln(\delta_D)]$, and the thin lines show the confidence band corresponding to the mean prediction $\pm\sigma_1$ and σ_2. For the 3D analysis, the unknown parameters in Eq. (2.4) for $k = x$ and $k = y$ are set to be equal due to the symmetry of the structure. Table 3.2 provides the posterior statistics of the unknown parameters in Eq. (2.4). Figure 3.11 shows the demand models in the x (left plot) and y (right plot) directions. As in Figure 3.10, the dots (•) and the open circles (○) show the measured logarithm of the maximum drift, corresponding to $\ln(S_{ak}) \le \theta_{S_a k}$ and $\ln(S_{ak}) > \theta_{S_a k}$, respectively. The thick lines represent the mean prediction $E[\ln(\delta_{Dk})]$, and the thin lines show the confidence bands corresponding to the mean predictions $\pm\sigma_{1k}$ and σ_{2k}.

Table 3.1 Posterior statistics of the parameters in the bilinear demand model in Eq. (2.2)

Parameter	Mean	Standard Deviation	Correlation Coefficient					
			θ_0	θ_1	σ_1	θ_{Sa}	θ_2	σ_2
θ_0	1.15	0.05	1					
θ_1	0.99	0.02	0.97	1				
σ_1	0.13	0.01	0.11	0.11	1			
θ_{Sa}	-1.83	0.05	0.17	0.17	0.41	1		
θ_2	1.19	0.05	-0.23	-0.22	-0.05	0.08	1	
σ_2	0.36	0.03	-0.05	-0.04	0.22	0.04	0.05	1

Table 3.2 Posterior statistics of the parameters in the demand model in Eq. (2.4)

Parameter	Mean	Standard Deviation	Correlation Coefficient					
			θ_{0k}	θ_{1k}	σ_{1k}	θ_{Sak}	θ_{2k}	σ_{2k}
θ_{0k}	1.17	0.05	1					
θ_{1k}	1.01	0.01	0.98	1				
σ_{1k}	0.13	0.01	0.28	0.22	1			
θ_{Sak}	-1.82	0.11	0.24	0.22	0.62	1		
θ_{2k}	1.18	0.05	-0.23	-0.22	0.40	0.61	1	
σ_{2k}	0.35	0.04	0.25	0.24	0.52	0.72	0.44	1

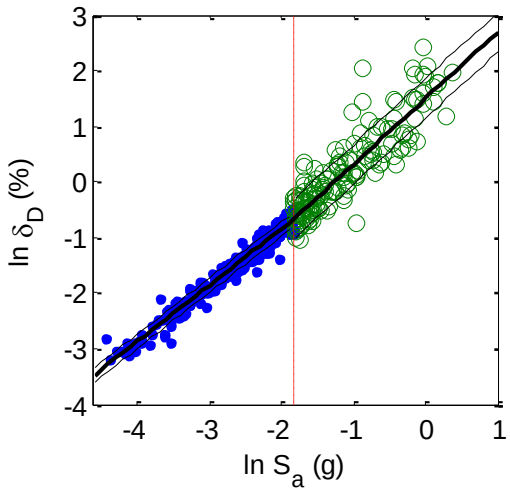

Figure 3.10 Bilinear demand model based on 2D response

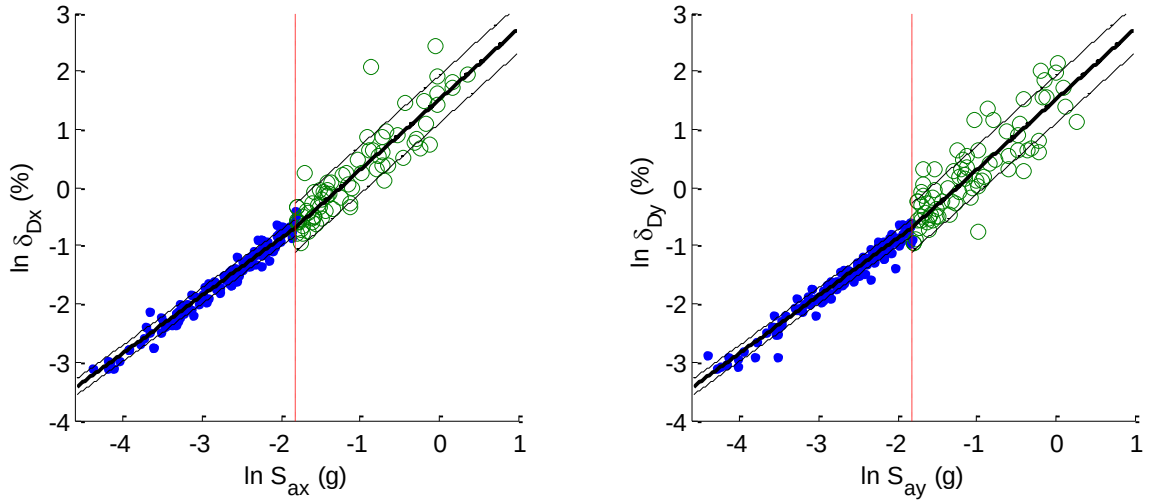

(a) x-direction **(b)** y-direction

Figure 3.11 Bilinear demand model fitting the measured drifts in the two planar directions

Table 3.3 provides the posterior statistics of the unknown parameters in the total demand model in Eq. (2.5). Figure 3.12 shows the measured and predicted total drift demands. The dots (•) show the value of $\ln(\delta_D)$ versus $\ln(\hat{\delta}_{SRSS})$ from the 3D time history analysis. The thick line represents the mean prediction $E[\ln(\delta_D)]$, and the thin lines show the confidence band corresponding to $E[\ln(\delta_D)] \pm \sigma_D$. Finally, Figure 3.13 shows the demand model contour, with respect to $\ln(S_{ax})$ and $\ln(S_{ay})$. The thick curves are the mean prediction $E[\ln(\delta_D)]$ and the thin curves show the confidence band corresponding to $E[\ln(\delta_D)] \pm \sigma_D$.

Table 3.3 Posterior statistics of the parameters in the total demand model in Eq. (2.5)

Parameter	Mean	Standard Deviation	Correlation Coefficient		
			θ_0	θ_1	σ
θ_0	0.07	0.02	1		
θ_1	0.91	0.01	0.46	1	
σ	0.30	0.01	0.00	0.00	1

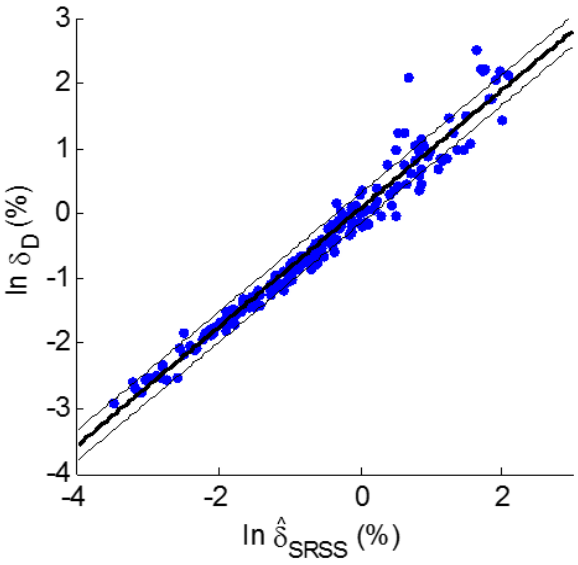

Figure 3.12 Total demand model fitting the measured drifts

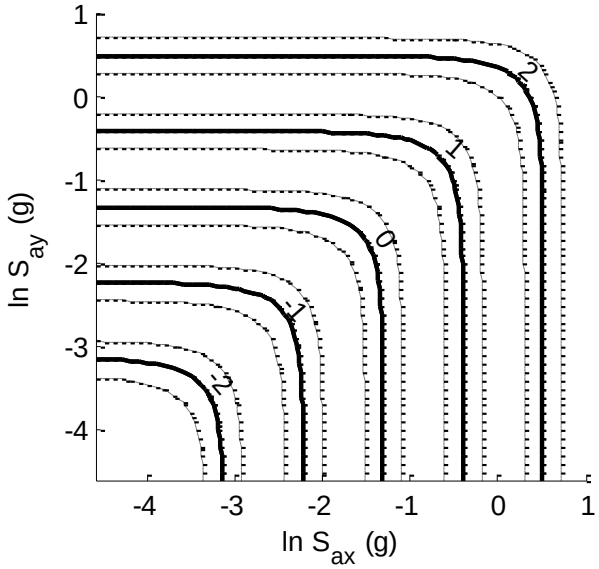

Figure 3.13 Bivariate demand model with respect to $\ln S_{ay}$ and $\ln S_{ax}$

CHAPTER 4

PROPOSED DRIFT CAPACITY MODEL FOR 3D RESPONSE OF RC COLUMNS

Structural capacity is generally defined as the response of the structure when reaching a given performance level [11]. Two types of performance levels are commonly used to determine the capacity. The first type is based on the results of a pushover analysis and it includes the following two performance levels: First Yield (FY) and Plastic Mechanism Initiation (PMI) [11]. Table 4.1 provides the descriptions for these performance levels. The second type, adopted by FEMA 356 [21] and ASCE/SEI 41-06 [22], includes three performance levels defined based on four damage states. The three performance levels are: Immediate Occupancy (IO), Life Safety (LS) and Collapse Prevention (CP). Table 4.2 provides the descriptions for these performance levels and corresponding damage states proposed by Bai et al. [23]. The drift capacities for FY and PMI performance levels are typically determined by a 2D displacement-based pushover analysis [24, 25]. Similarly, the FEMA 356 [21] and ASCE/SEI 41-06 [22] code provide the drift capacities for IO, LS and CP based on 2D responses.

Table 4.1 Description for the performance levels FY and PMI

Performance Level	Description
FY	One member of a story initiates yielding under imposed lateral loads.
PMI	A story mechanism initiates under imposed lateral loads

Table 4.2 Description for the performance levels IO, LS and CP, and the corresponding damage states

Performance Level	Damage State	Description
IO→	Insignificant	Damage requires no more than cosmetic repair. No structural repairs are necessary.
LS→	Moderate	The structure retains the pre-earthquake design stiffness and strength, and remains safe to occupy.
CP→	Heavy	The structure can retain a margin against onset of partial or total collapse, though there is damage to the components.
	Complete	The structure can continue to support the gravity loads, but it cannot retain any margin against collapse

However, the 2D analyses neglect the strength and stiffness degradation due to the bi-axial loading effects [26, 27]. So they tend to overestimate the capacity of the structure. This paper proposes to carry out 3D pushover analyses to determine the capacities for FY and PMI. The 3D pushover analyses increase the displacements in the two planar directions simultaneously. The ratio between the displacement increments in the two planar directions is kept constant within each analysis. To explore the differences in the responses, four ratios of the displacement increments in the two planar directions are considered. Specifically, by changing $\omega = \arctan(\delta_x / \delta_y)$, we obtain the capacities for FY and PMI with respect to different ω's. Capacities for IO, LS and CP cannot be obtained directly, because they are defined based on the specific damage states. This study computes these values by shifting the capacities for IO, LS and CP provided in ASCE/SEI 41-06 [22] (i.e., $\omega = 0^o$) by an amount equal to the linear interpolation between the shifts in the capacities for FY and PMI from 3D pushover analyses.

Figure 4.1 shows the pushover curves and the capacities with respect to four ω's (ω equal to

0^o, 15^o, 30^o and 45^o). The left plot in Figure 4.1 gives the pushover curves corresponding to the four ω's. The right plot shows the capacities for the five performance levels for each ω. Figure 4.2 shows the relationship between the drift capacity (δ_C) and ω for the five performance levels, where ω is in the range $[0^o, 45^o]$. The pushover curves and capacities for $90^o - \omega$ are the same as those for ω, due to the symmetry of the structure.

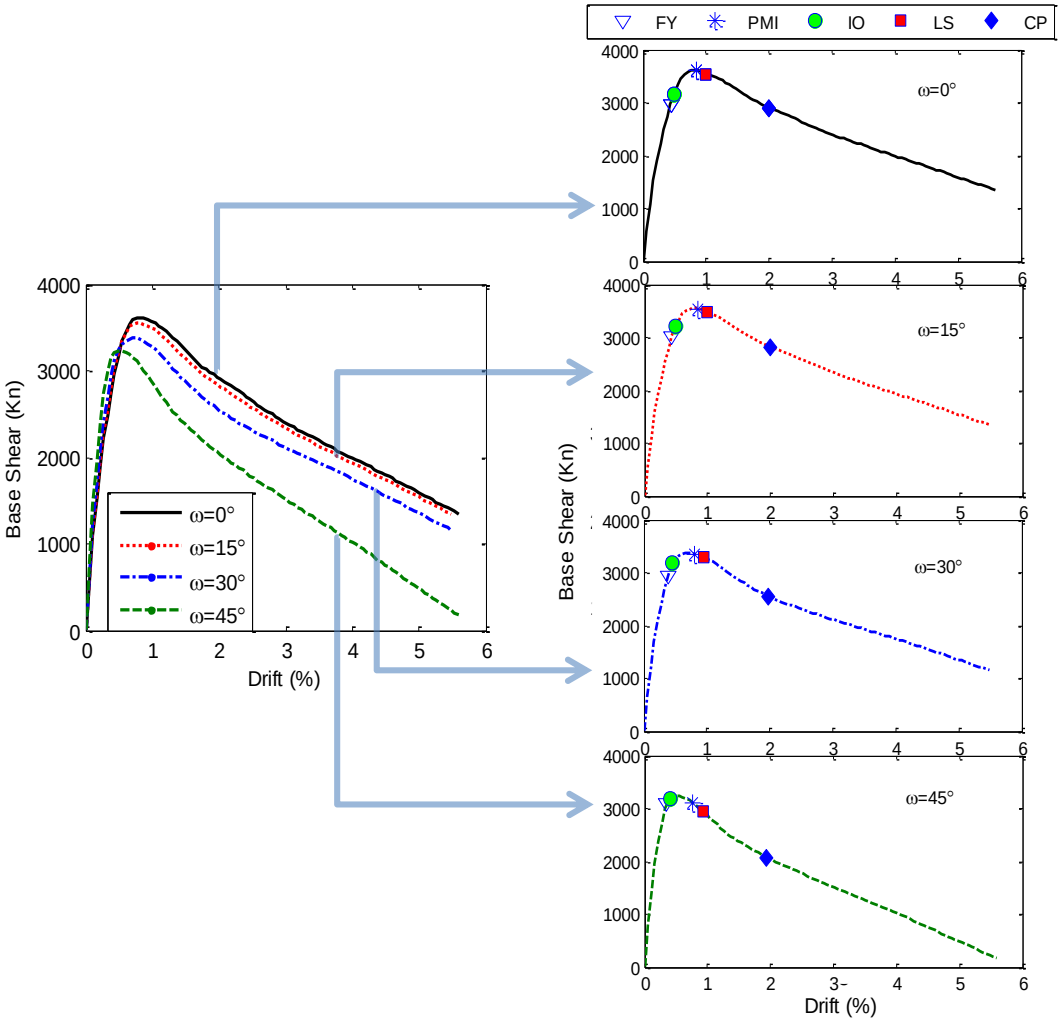

Figure 4.1 Pushover curves and capacities for four response angles

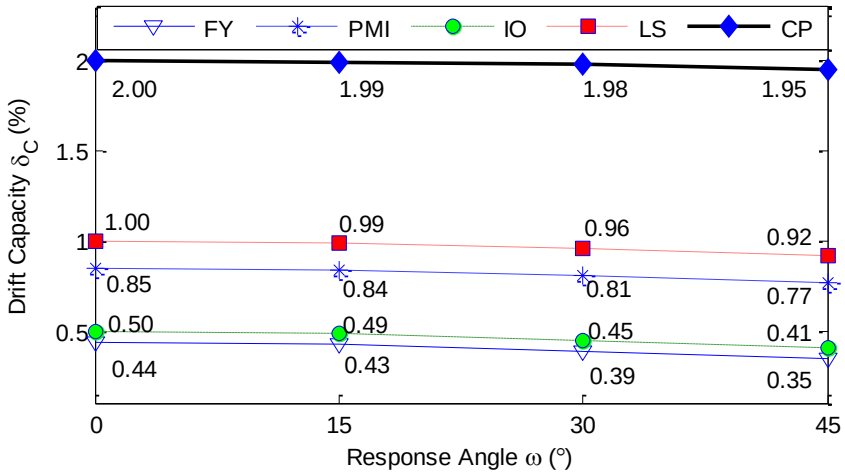

Figure 4.2 Relationship between drift capacity and response angle

From Figure 4.1 and 4.2, it can be seen that the structural response and the capacity vary with ω. The difference among the structural responses is especially obvious in the plastic response range. The capacities decrease with ω going from 0^o to 45^o for all five performance levels. These decreases as ω increases are due to the reduction in the cross-sectional moment of inertia and the increase of the distance between the outer fiber in tension and the neutral axis. Because ω changes randomly during an earthquake and in between earthquakes, we construct fragility estimates by comparing the predicted demand with both the maximum and minimum values of the capacity for each performance level.

CHAPTER 5

THREE-DIMENSIONAL FRAGILITY ESTIMATES

5.1 Seismic Fragility Estimates of the RC Building

An approximate estimate of the median fragility for both 2D and 3D analyses can be formulated generalizing the 2D formulation in Wen et al. [11] as:

$$F\left(\mathbf{S}_a;\boldsymbol{\Theta}\right) \cong 1-\Phi\left(\frac{\lambda_C-\lambda_{D|\mathbf{S}_a}\left(\mathbf{S}_a;\boldsymbol{\theta}\right)}{\sqrt{\sigma_{D|\mathbf{S}_a}^2+\sigma_C^2+\sigma_m^2}}\right) \tag{5.1}$$

where $\mathbf{S}_a = S_a$ for the 2D analysis and $\mathbf{S}_a = (S_{ax}, S_{ay})$ for the 3D analysis; $\lambda_C = E[\ln(\delta_C)]$; $\lambda_{D|\mathbf{S}_a} = E[\ln(\delta_D)]$; $\sigma_{D|\mathbf{S}_a}$ is the standard deviation of the demand model; σ_C and σ_m represent the uncertainties in the capacity and modeling, respectively. Following the recommendations of Wen et al. [11] , both σ_C and σ_m are assumed to be equal to 0.3. Following Gardoni et al. [12], a point estimate of the fragility can be found using point estimates of $\boldsymbol{\Theta}$ in Eq. (5.1). Specifically, if the mean values, $\mathbf{M}_{\boldsymbol{\Theta}}$, of $\boldsymbol{\Theta}$ are used, then Eq. (5.1) gives the median of the fragility estimate.

To reflect the influence of the statistical uncertainty in the estimates of $\boldsymbol{\Theta}$ on the fragility estimates, we can construct confidence bounds following Gardoni et al. [12] as:

$$\left\{\Phi\left[-\beta(\mathbf{S}_a)-\sigma_\beta(\mathbf{S}_a)\right], \Phi\left[-\beta(\mathbf{S}_a)+\sigma_\beta(\mathbf{S}_a)\right]\right\} \tag{5.2}$$

where

$$\beta(\mathbf{S}_a) = \left. \frac{\lambda_C - \lambda_{D|\mathbf{S}_a}(\mathbf{S}_a;\boldsymbol{\theta})}{\sqrt{\sigma^2_{D|\mathbf{S}_a} + \sigma^2_C + \sigma^2_m}} \right|_{\boldsymbol{\Theta}=\mathbf{M}_{\boldsymbol{\Theta}}} \tag{5.3}$$

$$\sigma^2_\beta(\mathbf{S}_a) \approx \nabla_{\boldsymbol{\Theta}}\beta(\mathbf{S}_a)\big|_{\boldsymbol{\Theta}=\mathbf{M}_{\boldsymbol{\Theta}}} \Sigma_{\boldsymbol{\Theta}\boldsymbol{\Theta}} \nabla_{\boldsymbol{\Theta}}\beta(\mathbf{S}_a)^T\Big|_{\boldsymbol{\Theta}=\mathbf{M}_{\boldsymbol{\Theta}}} \tag{5.4}$$

in which $\nabla_{\boldsymbol{\Theta}}\beta(\mathbf{S}_a)|_{\boldsymbol{\Theta}=\mathbf{M}_{\boldsymbol{\Theta}}}$ is the gradient of $\beta(\mathbf{S}_a;\boldsymbol{\Theta})$ computed at $\mathbf{M}_{\boldsymbol{\Theta}}$; $\Sigma_{\boldsymbol{\Theta}\boldsymbol{\Theta}}$ is the covariance matrix of $\boldsymbol{\Theta}$.

When constructing fragility estimates based on a 3D analysis, it is also important to know the typical range of one of the two spectral accelerations with respect to the other one to define the likely domain of the variables in the (S_{ax}, S_{ay})-space. This paper uses a linear model to show this relationship, which is as follows:

$$\ln(S_{ay}) = \alpha_0 + \alpha_1 \ln(S_{ax}) + \sigma_S \varepsilon \tag{5.5}$$

where $\alpha_0 = 0$ and $\alpha_1 = 1$ to reflect that with no knowledge on the specific site any direction is equally likely, and $\sigma_S\varepsilon =$ the model error, where σ_S is the unknown constant standard deviation and ε is a standard normal random variable. Using the ground motions used to calibrate the demand models, the mean and standard deviation of σ_S are 0.43 and 0.02, respectively.

Figures 5.1-5.5 show the fragility estimates for the building shown in Figure 3.1, with respect to the five performance levels. In each figure, the left plots consider the maximum capacity and the right plots consider the minimum capacity. Plot (a) shows the contour of the fragility surface in terms of S_{ax} and S_{ay} for the 3D analysis. The solid straight line is the median S_{ay} with respect

to S_{ax}, and the dash lines are the one standard deviation confidence bounds of S_{ay} considering σ_S. Plot (b) shows the median fragility versus S_{ax}. This plot provides three fragility curves from the 3D analysis and one curve from the 2D analysis. The three curves for the 3D analysis are derived using S_{ay} equal to its median value, S_{ax}, (thick line), and its upper and lower bound values (thin lines) obtained from Eq. (5.5). Plot (c) shows the median fragility versus S_{ax} and the confidence bounds of the fragility computed using Eq. (5.2). For the fragility based on the 3D analysis, the fragility and bounds are for $S_{ay} = S_{ax}$.

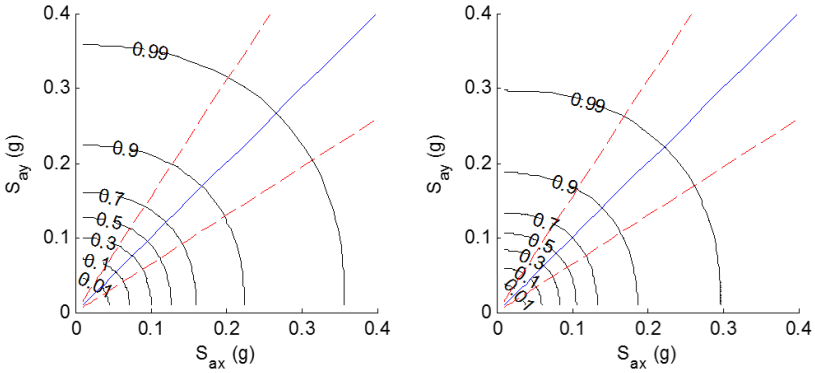

(a) Fragility contour in terms of S_{ax} and S_{ay}

(Solid and dash straight lines are the median and bounds of S_{ay}, respectively)

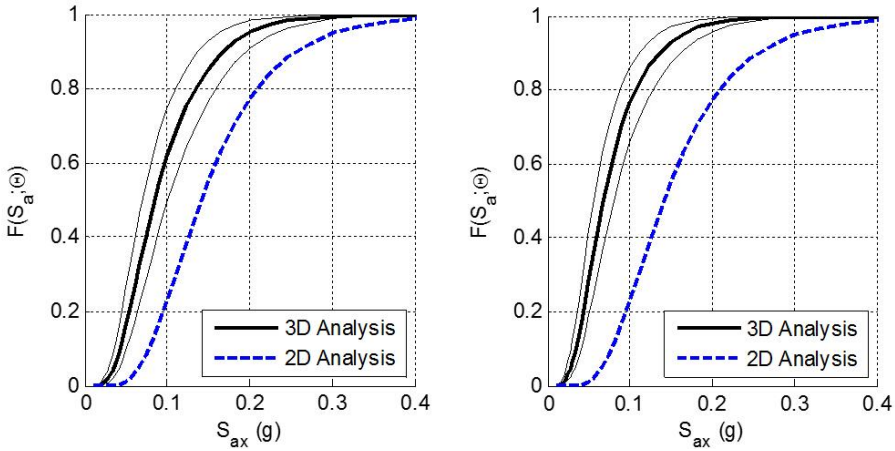

(b) Median fragility curves in 3D and 2D analysis

(Thick lines consider the median S_{ay}; thin lines consider the upper and lower bound of S_{ay})

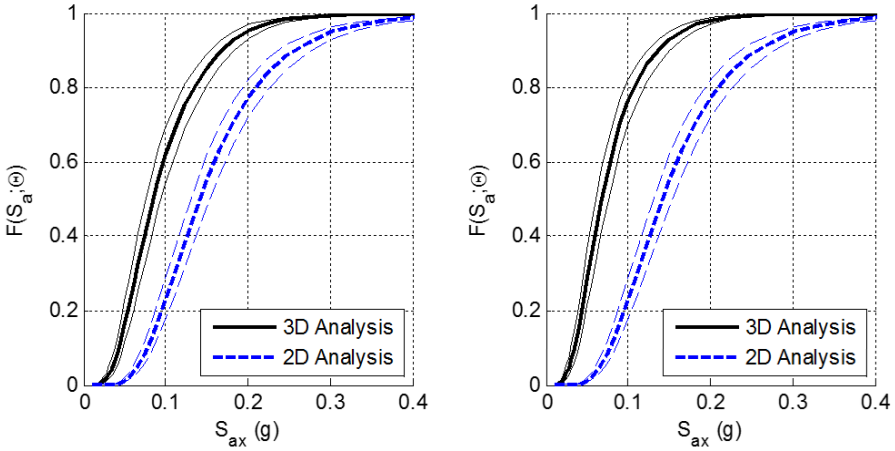

(c) Confidence bounds of the fragility in 3D and 2D analysis

(Thick lines are the median fragility; thin lines are the corresponding confidence bounds)

Figure 5.1 Fragility estimates for FY (left for max. capacity; right for min. capacity)

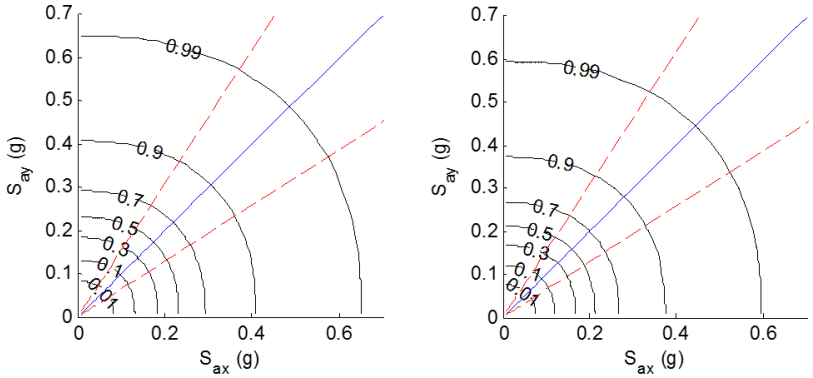

(a) Fragility contour in terms of S_{ax} and S_{ay}

(Solid and dash straight lines are the median and bounds of S_{ay}, respectively)

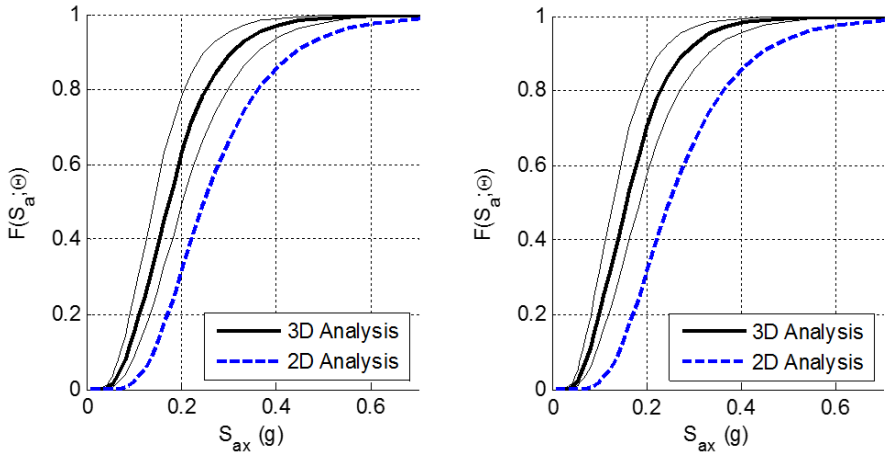

(b) Median fragility curves in 3D and 2D analysis

(Thick lines consider the median S_{ay}; thin lines consider the upper and lower bound of S_{ay})

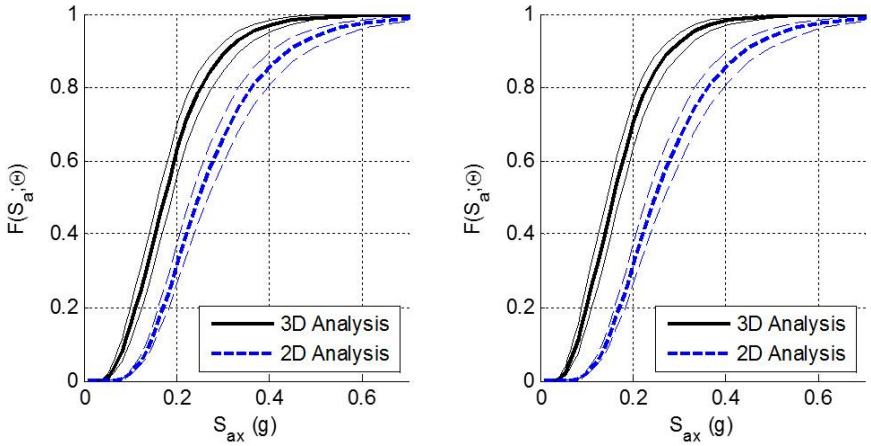

(c) Confidence bounds of the fragility in 3D and 2D analysis

(Thick lines are the median fragility; thin lines are the corresponding confidence bounds)

Figure 5.2 Fragility estimates for PMI (left for max. capacity; right for min. capacity)

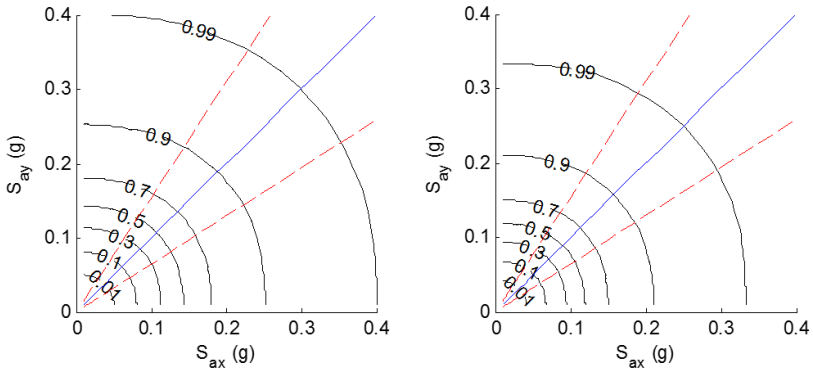

(a) Fragility contour in terms of S_{ax} and S_{ay}

(Solid and dash straight lines are the median and bounds of S_{ay}, respectively)

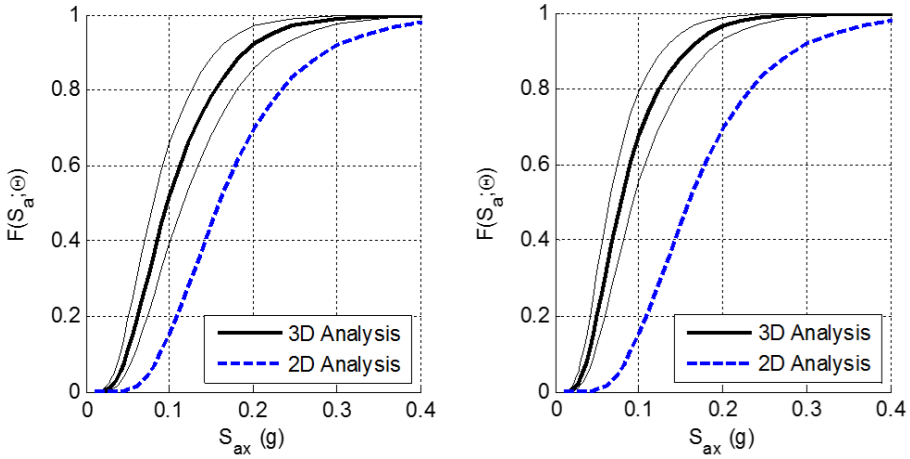

(b)Median fragility curves in 3D and 2D analysis

(Thick lines consider the median S_{ay}; thin lines consider the upper and lower bound of S_{ay})

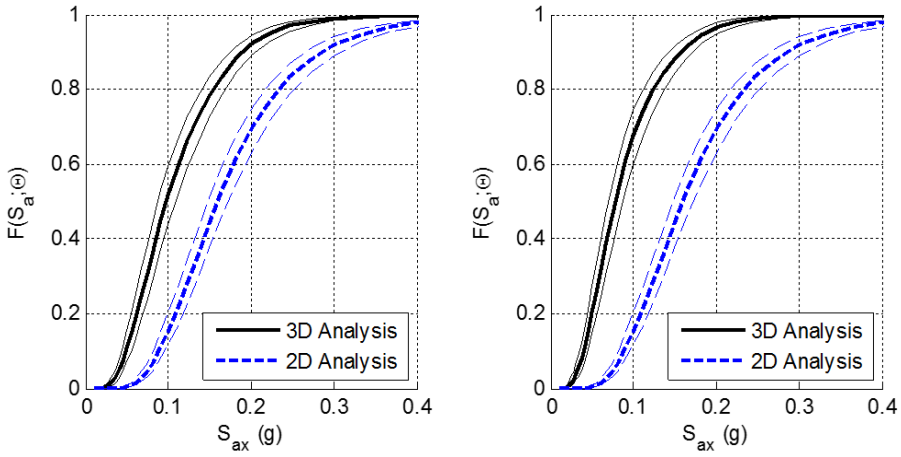

(c) Confidence bounds of the fragility in 3D and 2D analysis

(Thick lines are the median fragility; thin lines are the corresponding confidence bounds)

Figure 5.3 Fragility estimates for IO (left for max. capacity; right for min. capacity)

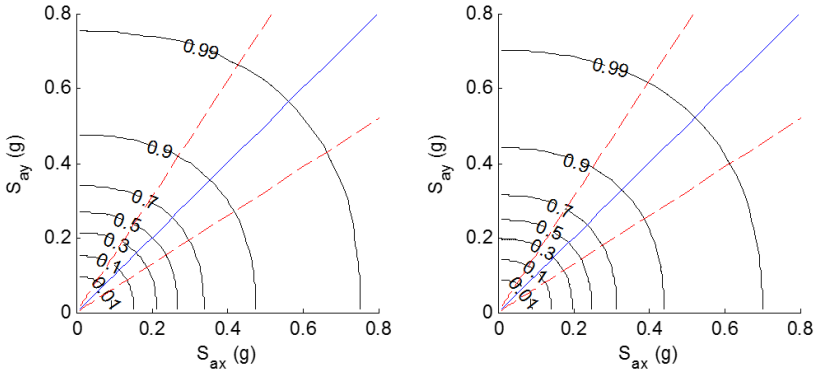

(a) Fragility contour in terms of S_{ax} and S_{ay}

(Solid and dash straight lines are the median and bounds of S_{ay}, respectively)

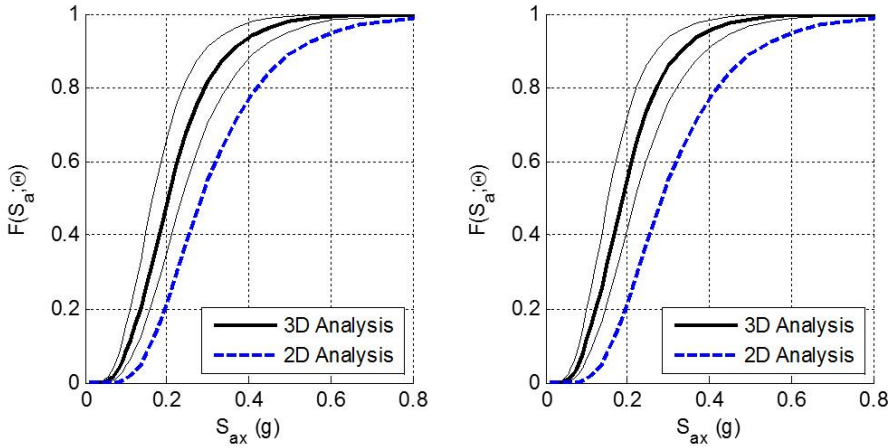

(b) Median fragility curves in 3D and 2D analysis

(Thick lines consider the median S_{ay}; thin lines consider the upper and lower bound of S_{ay})

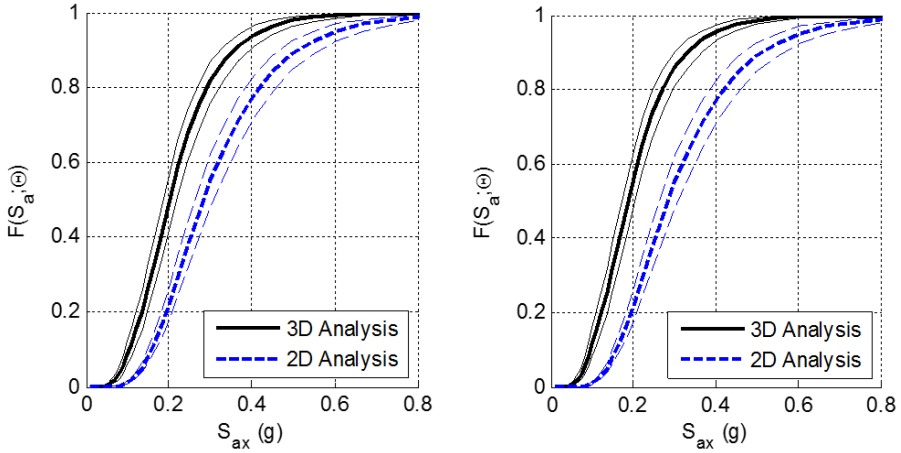

(c) Confidence bounds of the fragility in 3D and 2D analysis

(Thick lines are the median fragility; thin lines are the corresponding confidence bounds)

Figure 5.4 Fragility estimates for LS (left for max. capacity; right for min. capacity)

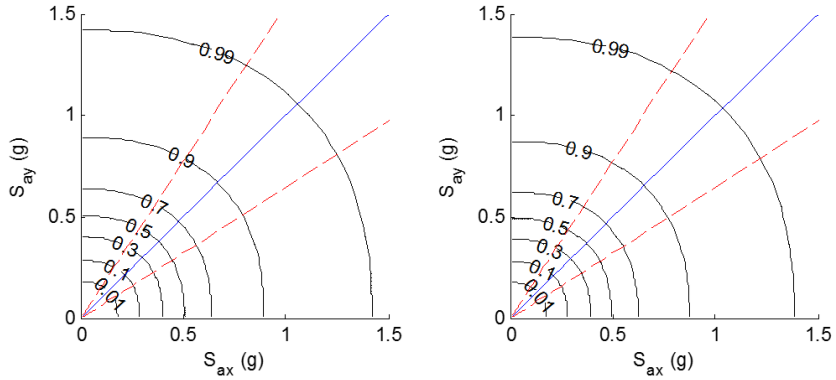

(a) Fragility contour in terms of S_{ax} and S_{ay}

(Solid and dash straight lines are the median and bounds of S_{ay}, respectively)

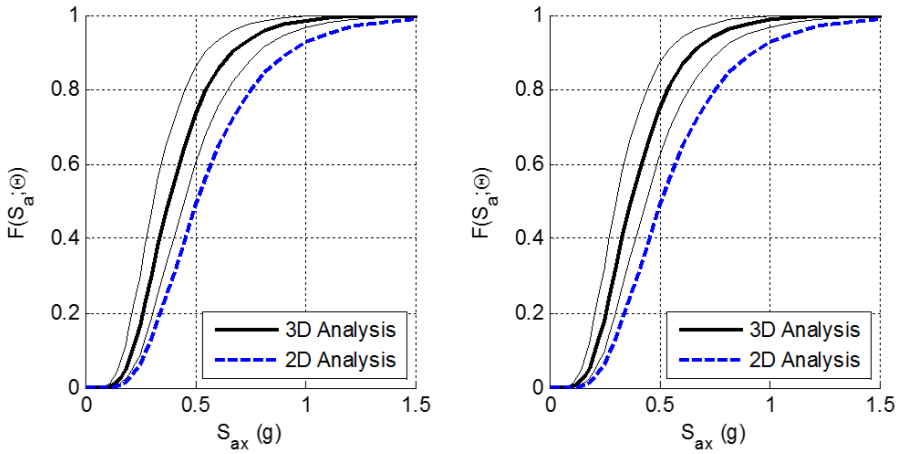

(b) Median fragility curves in 3D and 2D analysis

(Thick lines consider the median S_{ay}; thin lines consider the upper and lower bound of S_{ay})

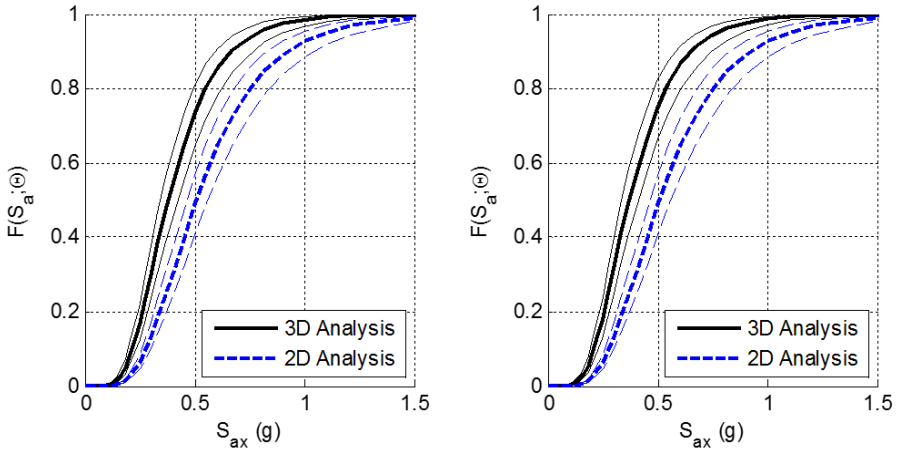

(c) Confidence bounds of the fragility in 3D and 2D analysis

(Thick lines are the median fragility; thin lines are the corresponding confidence bounds)

Figure 5.5 Fragility estimates for CP (left for max. capacity; right for min. capacity)

5.2 Observations from the 2D and 3D Fragility Estimates

From Plots (a) and (b) in Figures 5.1-5.5, it can be seen that the fragilities computed by considering S_{ay} equal to its median value (i.e., S_{ax}) and its upper and lower bound values are significantly different. Specifically, the range of fragility estimates computed based on the lower bound and the upper bound of S_{ay} is quite broad. This indicates that the possible range of S_{ay} with respect to a given S_{ax} has a significant effect on the fragility. The same can be said in regard to the effects of the possible range of S_{ax} with respect to a given S_{ay}. In addition, all the fragility estimates based on the 3D analysis are higher than the ones based on the 2D analysis (as shown in Plots (b)) even when the fragility based on the 3D analysis consider the lower bound of S_{ay} for a given S_{ax}. This means the 2D analysis underestimates the fragility compared with the more realistic 3D analysis that considers the effects of both S_{ax} and S_{ay} on the structural responses.

From Plots (c), we can see that the confidence bands in the 3D and 2D fragility analysis have similar widths. This means that the effect on the fragility estimates of the model uncertainty involved in the 3D analysis is close to the one in the 2D analysis. For each performance level, the lower bound of the fragility based on the 3D analysis is higher than the upper bound of the fragility based on the 2D analysis. This also indicates that the 2D analysis heavily underestimates the fragility compared to the 3D analysis.

When comparing the left plots (maximum capacity) with the right plots (minimum capacity) in each of the Figures 5.1-5.5, it can be seen that the fragility considering the maximum capacity is

slightly lower than the one considering the minimum capacity. This indicates that the effect on the fragility estimates of changes in the capacity are less significant than the changes due to the variability in S_{ay} for a given S_{ax}.

CONCLUSION

This study proposed an approach to estimate the seismic fragility of the RC buildings based on two horizontal spectral accelerations (S_{ax} and S_{ay}). This approach compares the drift demand with the corresponding structural capacity based on the three-dimensional (3D) structural response.

The drift demand models used in previous 2D analysis do not consider the effects of the bi-axial ground motion excitation. To account for the effects of bi-axial loadings on the structural response, this study used a bivariate demand model, which is a function of S_{ax} and S_{ay}.

In addition, the traditional planar analysis, such as two-dimensional (2D) pushover analysis, does not consider the capacity variation due to the change in the response angle, ω, which might overestimate the drift capacity. This study proposed to conduct 3D pushover analysis to obtain the drift capacity with respect to ω. This study considered the capacities for five performance levels, namely, First Yield (FY), Plastic Mechanism Initiation (PMI), Immediate Occupancy (IO), Life Safety (LS), and Collapse Prevention (CP).

Next, this study constructed 3D fragility estimates using the proposed demand and capacity models. The formulation is illustrated considering a symmetric RC frame building. The result shows that the current 2D analyses heavily underestimate the fragility compared with those obtained based on the proposed 3D analysis. The variability in S_{ay} with respect to a given S_{ax}, has a significant effect on the fragility estimates. Confidence bands computed for the 2D and 3D analysis are similar,

which indicates that the statistical uncertainty in the 2D and 3D analysis is comparable. Finally, it is observed that the change of capacity also affects the fragility estimates, but in a less significant way than the change due to the variability in S_{ay} for a given S_{ax}.

REFERENCES

[1] Hwang HH, Low YK. Seismic reliability analysis of plane frame structures. Probabilistic Engineering Mechanics. 1989;4:74-84.

[2] Erberik MA, Elnashai AS. Fragility analysis of flat-slab structures. Engineering Structures. 2004;26:937-48.

[3] Ramamoorthy SK, Gardoni P, Bracci JM. Probabilistic demand models and fragility curves for reinforced concrete frames. Journal of Structural Engineering. 2006;132:1563-72.

[4] Ramamoorthy SK, Gardoni P, Bracci JM. Seismic fragility and confidence bounds for gravity load designed reinforced concrete frames of varying height. Journal of Structural Engineering. 2008;134:639-50.

[5] Ellingwood BR, Celik OC, Kinali K. Fragility assessment of building structural systems in Mid-America. Earthquake Engineering & Structural Dynamics. 2007;36:1935-52.

[6] Celik OC, Ellingwood BR. Seismic risk assessment of gravity load designed reinforced concrete frames subjected to Mid-America ground motions. Journal of Structural Engineering. 2009;135:414-24.

[7] Bai J-W, Gardoni P, Hueste MBD. Story-specific demand models and seismic fragility estimates for multi-story buildings. Structural Safety. 2011;33:96-107.

[8] Schotanus M, Franchin P, Lupoi A, Pinto P. Seismic fragility analysis of 3D structures. Structural Safety. 2004;26:421-41.

[9] Jeong S-H, Elnashai AS. New three-dimensional damage index for RC buildings with planar irregularities. Journal of Structural Engineering. 2006;132:1482-90.

[10] Aziminejad A, Moghadam A. Fragility-based performance evaluation of asymmetric single-story buildings in near field and far field earthquakes. Journal of Earthquake Engineering. 2010;14:789-816.

[11] Wen YK, Ellingwood BR, Bracci JM. Vulnerability function framework for consequence-based engineering, Mid-American Earthquake Center Project DS-4 Report, University of Illinois at Urbana-Champaign, Illinois; 2004.

[12] Gardoni P, Der Kiureghian A, Mosalam KM. Probabilistic capacity models and fragility estimates for reinforced concrete columns based on experimental observations. Journal of Engineering Mechanics. 2002;128:1024-38.

[13] Simon J, Bracci JM, Gardoni P. Seismic response and fragility of deteriorated reinforced concrete bridges. Journal of Structural Engineering. 2010;136:1273-81.

[14] ACI Committee. Building code requirements for structural concrete and commentary. ACI-318: American Concrete Institution; 2002.

[15] McKenna F, Fenves G, Scott M. Open system for earthquake engineering simulation. University of California, Berkeley, California. 2000.

[16] PEER Strong motion database. < http://peer.berkeley.edu/smcat >; 2000.

[17] Shome N, Cornell CA. Probabilistic seismic demand analysis of nonlinear structures. Reliability of Marine Structures Report No. RMS-35, Department of Civil and Environmental Engineering, Stanford University, Stanford, California; 1999.

[18] Abrahamson N, Silva W. Empirical response spectral attenuation relations for shallow crustal earthquakes. Seismological Research Letters. 1997;68:94-127.

[19] Box GE, Tiao GC. Bayesian inference in statistical analysis: John Wiley & Sons; 2011.

[20] Laine M. Adaptive MCMC methods with applications in environmental and geophysical models. PhD thesis. Lappeenranta University of Technology, Lappeenranta, Finland; 2008.

[21] FEMA. Prestandard and commentary for the seismic rehabilitation of buildings. FEMA 356, ASCE. Reston, Virginia; 2000.

[22] ASCE/SEI. Seismic rehabilitation of existing buildings. ASCE/SEI 41-06. Reston, Virginia; 2007.

[23] Bai J-W, Hueste MBD, Gardoni P. Probabilistic assessment of structural damage due to earthquakes for buildings in Mid-America. Journal of Structural Engineering. 2009;135:1155-63.

[24] Dooley KL, Bracci JM. Seismic evaluation of column-to-beam strength ratios in reinforced concrete frames. ACI Structural Journal. 2001; 99:843-851.

[25] Mwafy A, Elnashai A. Static pushover versus dynamic collapse analysis of RC buildings. Engineering Structures. 2001;23:407-24.

[26] Rodrigues H, Varum H, Arêde A, Costa A. Comparative efficiency analysis of different nonlinear modelling strategies to simulate the biaxial response of RC columns. Earthquake Engineering and Engineering Vibration. 2012;11:553-66.

[27] Rodrigues H, Arêde A, Varum H, Costa AG. Experimental evaluation of rectangular reinforced concrete column behaviour under biaxial cyclic loading. Earthquake Engineering & Structural Dynamics. 2013;42:239-59.